Journal of Quantitative Spectroscopy & Radiative Transfer 113 (2012) 1913–1919

Contents lists available at SciVerse ScienceDirect

Journal of Quantitative Spectroscopy & Radiative Transfer

journal homepage: www.elsevier.com/locate/jqsrt

Measurements of the infrared absorption cross-sections of HCFC-141b (CH_3CFCl_2)

Karine Le Bris [a,*], James McDowell [a], Kimberly Strong [b]

[a] Department of Physics, St. Francis Xavier University, P.O. Box 5000, Antigonish, NS, Canada B2G 2W5
[b] Department of Physics, University of Toronto, 60 St. George Street, Toronto, Ontario, Canada M5S 1A7

ARTICLE INFO

Article history:
Received 9 March 2012
Received in revised form
2 May 2012
Accepted 3 May 2012
Available online 15 May 2012

Keywords:
Hydrochlorofluorocarbon
HCFC-141b
Cross-section
Mid-infrared
FTIR
Gas phase
Temperature-dependence
Integrated band intensity
Ab initio
Density functional theory

ABSTRACT

Detection of atmospheric trace gases by optical remote sensing techniques relies on the availability of molecular absorption spectra over a range of relevant temperatures. Absorption cross-sections of a pure vapour of the hydrochlorofluorocarbon HCFC-141b are reported at a resolution of 0.02 cm^{-1} for a range of temperatures between 223 and 283 K and a spectral range of 570–3100 cm^{-1}. The integrated intensities of the nine main harmonic bands compare well with the data available from previous experimental studies and with theoretical calculations by ab initio and density functional theories.

1. Introduction

After the phase-out of chlorofluorocarbons by the Montreal Protocol and its further amendments, HCFC-141b (1,1-dichloro-1-fluoroethane or CH_3CFCl_2) has been extensively used to replace CFC-113 as a solvent, and CFC-11 as a foam-blowing agent in manufacturing processes. Its concentration in the atmosphere has risen quickly from the early 1990s to reach a mean global surface mixing ratio above 22 ppt (part per trillion) at the end of 2011 [1]. HCFC-141b is currently the second most abundant hydrochlorofluorocarbon in the atmosphere after HCFC-22 ($CHClF_2$).

Measurements of HCFC-141b have recently been reported from space-borne missions [2]. An important factor for data retrieval is the quality of the spectroscopic information available over a range of relevant atmospheric temperatures. The purpose of this study is to provide new infrared absorption cross-section spectra of pure HCFC-141b from 223 to 283 K at a resolution of 0.02 cm^{-1} (OPD = 50 cm).

2. Experimental set-up

Experimental data are acquired using Fourier transform infrared (FTIR) absorption spectroscopy. The Fourier transform spectrometer (FTS) is a Bomem DA8.002 equipped with a KBr beamsplitter and operating with a Globar source.

The gas sample (Synquest Laboratories, 99.5%) is contained in a stainless steel cell positioned between the FTS and a liquid nitrogen-cooled mercury cadmium telluride (MCT) detector. ZnSe windows are sealed to the gas cell

* Corresponding author. Tel: +1 902 867 2392; fax: +1 902 867 2414.
E-mail address: klebris@stfx.ca (K. Le Bris).

0022-4073/$ - see front matter © 2012 Elsevier Ltd. All rights reserved.
http://dx.doi.org/10.1016/j.jqsrt.2012.05.004

with indium o-rings to prevent leakage at low temperature. A short pathlength of 2.93 cm has been chosen to avoid saturation effects while working at manageable pressures. HCFC-141b being liquid at room temperature, each sample is degassed by several Freeze-Pump-Thaw cycles prior to entering the cell. The cell pressure is measured by 10 Torr and 1000 Torr MKS baratron pressure gauges. All the acquisitions have been made with a pure vapour to allow a better accuracy of the pressure reading. Atmospheric retrievals can be performed with these laboratory cross-sections using the pseudo-lines method [3].

The cooling is achieved by a Neslab ULT-80 chiller sending the coolant (Syltherm XLT) to a copper tube surrounding the cell. The copper tube is soldered to the cell and covered by thermally conductive epoxy to enhance temperature homogeneity. The cell temperature is measured by a single thermocouple directly inserted inside the cell. The temperature readout accuracy during experiments is typically ± 0.1 °C for temperatures down to 263 K and ± 0.2 °C for lower temperatures.

Typical artefacts and sources of errors of FTIR spectra (i.e. spectral aliasing, dynamic alignment error, blackbody emission from the source aperture, and nonlinearity of the MCT detector in the mid-infrared) have been minimized using the same procedure as described in [4]. The spectral calibration of the instrument has been verified by comparing a laboratory CO_2 spectrum with the corresponding lines in the HITRAN 2008 database [5]. The average shift on the 50 lines we analyzed was negligible (-1.14×10^{-4} cm^{-1} with a standard deviation of 1.135×10^{-3} cm^{-1}).

3. Data analysis

For each temperature, a series of unapodised scans has been recorded at five pressures between 2 and 50 Torr for 283, 273, 263 and 253 K. The saturation vapour pressure of HCFC-141b limited the acquisitions at high pressure to 30 Torr at 243 K, 20 Torr at 233 K and 10 Torr at 223 K. Each pressure–temperature (P–T) spectrum is composed of a minimum of 200 unapodised scans.

Control baseline spectra, each of them generated from a minimum of 20 scans, are recorded before and after each sample measurements to account for the small intensity variations that can occur during the acquisitions. For each temperature, a several hundred scan primary baseline spectrum with high signal-to-noise ratio is produced from the multiple control baseline spectra. If need be, for each P–T acquisitions, the primary baseline spectrum can be adjusted to the control baseline spectra using a polynomial regression prior to the rationing of the sample spectrum to the background spectrum.

The cross-section, $\sigma(\nu)$, in cm^2/molecule is obtained using the Beer–Lambert law:

$$I(\nu) = I_0(\nu)e^{-\chi(\nu)}, \tag{1}$$

where ν is the wavenumber (cm^{-1}); I_0, the light intensity passing through the empty cell (baseline); I, the light intensity passing through the sample gas cell and χ, the optical depth defined by:

$$\chi(\nu) = \sigma(\nu)\frac{PT_0}{TP_0}N_L L. \tag{2}$$

N_L is Loschmidt's constant (2.6868×10^{19} molecules/cm^3); L, the length of the cell (cm); and P_0 and T_0, the standard conditions for pressure and temperature.

To prevent saturation effects in an optically thick medium while keeping a good signal-to-noise ratio at every wavenumber, the points corresponding to optically thick ($\chi(\nu) > 1.1$) or optically thin ($\chi(\nu) < 0.1$) conditions are eliminated. This way, a linear behaviour is obtained for strong absorption bands from the low-pressure measurements while weak absorption features are represented by the high-pressure measurements.

The shapes of the sharp ro-vibrational transition lines, as well as the peaks of the Q-branches, are pressure-dependent due to collisional broadening. Therefore, the cross-section for a pure vapour cannot be directly obtained by a linear fit of the optical depth as a function

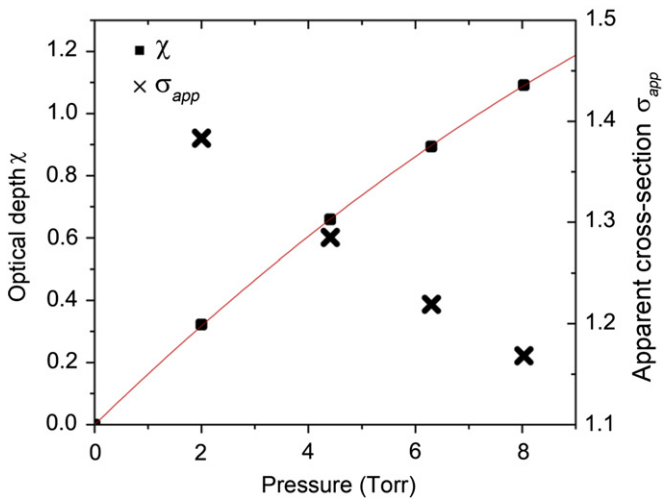

Fig. 1. Variation of the optical depth χ and apparent cross-section σ_{app} ($\times10^{-18}$ cm^2/molecule) as a function of pressure at $\nu = 752.963$ cm^{-1} for a temperature of 243 K. Note that the value at the highest pressure was not included in the calculation as its optical depth was higher than 1.1.

of the pressure. However, as illustrated in Fig. 1, the apparent cross-section σ_{app}, i.e. the cross-section obtained directly from the Beer–Lambert law for each temperature–pressure spectrum, varies linearly with pressure:

$$\sigma_{app} = a(\nu)P + b(\nu), \tag{3}$$

a and b being fitting coefficients.

The optical depth can, therefore, be written as

$$\chi(\nu) = \frac{T_0}{TP_0} N_L L[a(\nu)P + b(\nu)]P. \tag{4}$$

The real cross-section σ_{real}, i.e. the cross-section at the zero-Torr limit, is simply the fitting coefficient b retrieved through a quadratic fit of the optical depth.

All fits are performed with a forced convergence at $\chi(P=0)=0$. It has to be noted that optically thin media, such as the far wings of the bands, and optically thick media, such as the peaks of the Q-branches, may contain only one or two optical depths that fit inside the 0.1–1.1 interval. In such case, the cross-section is estimated through a linear fit of the optical depth to the pressure.

The integrated band intensities (in cm/molecule) are calculated by integrating the real cross-sections over the spectral range of each bands.

Systematic errors, ϵ_s, on the optical path length, temperature readout, and sample purity have been evaluated to be less than $\pm 3\%$. The other sources of error in spectral measurements come from a residual MCT non-linearity, a possible residual baseline drift, the pressure readout, the errors induced by the data reduction and the instrumental noise. These errors can all be accounted for through the standard deviation, ϵ_f, in the fit of the optical depth as a function of pressure. The uncertainty on the fit is chosen at the 95% confidence limit ($2\epsilon_f$). The total uncertainty presented below is the square root of the sum of ϵ_s and $2\epsilon_f$.

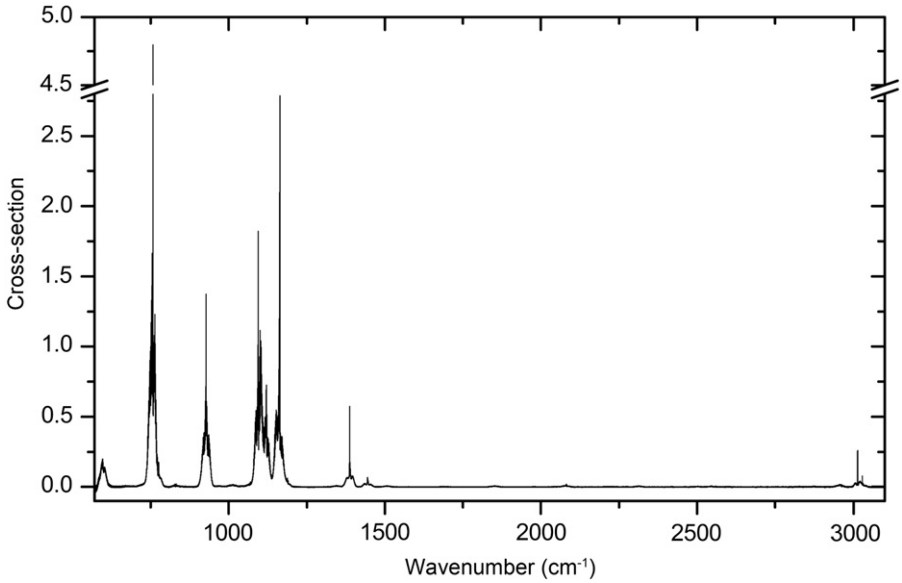

Fig. 2. Survey spectrum of HCFC-141b in the mid-infrared at 273 K. The cross-section unit is in $\times 10^{-18}$ cm^2/molecule.

Table 1
Theoretical harmonic wavenumbers and intensities of the fundamental modes of HCFC-141b. Wavenumbers are in cm^{-1}, integrated band intensities are in 10^{-17} cm/molecule. (a) B3LYP/cc-pVDZ, (b) MP2/cc-pVTZ.

Band	Assignment	Wavenumber		Integrated band intensity	
		(a)	(b)	(a)	(b)
570–630	ν_8	575.7546	603.3147	0.50778	0.35001
710–790	ν_{15}	712.6994	776.2470	3.22037	2.53595
895–955	ν_7	934.9084	955.8702	1.25336	1.06335
1030–1138	ν_{14}	1091.9475	1114.1503	3.11362	3.00897
	ν_6	1118.3837	1145.8577		
1138–1210	ν_5	1192.0780	1204.1752	1.94780	1.41671
1350–1420	ν_4	1393.0726	1414.1504	0.06018	0.32334
1420–1470	ν_{13}	1448.0726	1492.0384	0.26763	0.07575
	ν_3	1448.5282	1493.2170		
2920–2985	ν_2	3059.7446	3099.5403	0.03681	0.02142
2985–3055	ν_{12}	3145.0161	3199.6573	0.09113	0.05710
	ν_1	3169.4920	3216.2606		

Table 2
Comparison of the experimental infrared integrated band intensities ($\times 10^{-17}$ cm/molecule) of HCFC-141b with published values. The band range is in cm^{-1}. The first two set of [6] were acquired at 287 and 270 K. The two sets used from [7] are at 298 and 278 K.

Temperature	Band range	Integrated band intensity			
		Present work	Ref. [6]	Ref. [7]	Ref. [8]
295 K	570–630			0.332	0.335
	710–790			2.321	2.330
	895–955			1.072	1.085
	1030–1138			2.447	2.37
	1138–1210			1.416	1.395
	1350–1420			0.287	0.269
	1420–1470			0.081	0.08
	2920–2985			0.034	
	2985–3055			0.105	
283 K	570–630	0.380 ± 0.010			
	710–790	2.334 ± 0.073	2.375		
	895–955	1.071 ± 0.032	1.088		
	1030–1138	2.434 ± 0.075	2.485		
	1138–1210	1.404 ± 0.046	1.432		
	1350–1420	0.269 ± 0.008	0.268		
	1420–1470	0.075 ± 0.008	0.066		
	2920–2985	0.036 ± 0.008			
	2985–3055	0.109 ± 0.009			
273 K	570–630	0.321 ± 0.009		0.325	
	710–790	2.350 ± 0.076	2.218	2.313	
	895–955	1.059 ± 0.034	1.017	1.065	
	1030–1138	2.478 ± 0.083	2.358	2.442	
	1138–1210	1.419 ± 0.048	1.311	1.408	
	1350–1420	0.267 ± 0.011	0.243	0.286	
	1420–1470	0.074 ± 0.008	0.084	0.080	
	2920–2985	0.032 ± 0.011		0.033	
	2985–3055	0.106 ± 0.011		0.105	
263 K	570–630	0.364 ± 0.010			
	710–790	2.336 ± 0.075			
	895–955	1.040 ± 0.035			
	1030–1138	2.387 ± 0.081			
	1138–1210	1.385 ± 0.045			
	1350–1420	0.276 ± 0.009			
	1420–1470	0.077 ± 0.004			
	2920–2985	0.029 ± 0.006			
	2985–3055	0.104 ± 0.007			
253 K	570–630	0.344 ± 0.009			
	710–790	2.322 ± 0.075	2.160		
	895–955	1.050 ± 0.034	1.004		
	1030–1138	2.476 ± 0.076	2.118		
	1138–1210	1.415 ± 0.043	1.203		
	1350–1420	0.273 ± 0.010	0.247		
	1420–1470	0.075 ± 0.005	0.092		
	2920-2985	0.035 ± 0.010			
	2985–3055	0.114 ± 0.012			
243 K	570–630	0.311 ± 0.009			
	710–790	2.308 ± 0.076			
	895–955	1.037 ± 0.035			
	990–1138	2.403 ± 0.079			
	1138–1210	1.398 ± 0.043			
	1350–1420	0.276 ± 0.010			
	1420–1470	0.077 ± 0.005			
	2920–2985	0.034 ± 0.008			
	2985–3055	0.111 ± 0.009			
233 K	570–630	0.322 ± 0.009			
	710–790	2.324 ± 0.076			
	895–955	1.041 ± 0.034			
	1030–1138	2.507 ± 0.081			
	1138–1210	1.407 ± 0.044			

Table 2 (*continued*)

Temperature	Band range	Integrated band intensity			
		Present work	Ref. [6]	Ref. [7]	Ref. [8]
	1350–1420	0.274 ± 0.010			
	1420–1470	0.074 ± 0.004			
	2920–2985	0.030 ± 0.009			
	2985–3055	0.111 ± 0.010			
223 K	570–630	0.339 ± 0.009			
	710–790	2.397 ± 0.081			
	895–955	1.082 ± 0.038			
	1030–1138	2.457 ± 0.083			
	1138–1210	1.395 ± 0.049			
	1350–1420	0.278 ± 0.010			
	1420–1470	0.076 ± 0.003			
	2920–2985	0.029 ± 0.005			
	2985–3055	0.104 ± 0.005			

4. Experimental results

HCFC-141b is a near-prolate asymmetric top molecule belonging to the C_s symmetry group. Of its 18 fundamental vibration modes, 11 (ν_1–ν_{11}) are symmetric, and the rest (ν_{12}–ν_{18}) are antisymmetric. Twelve fundamental vibration modes have active absorption bands in the spectral region of interest.

As seen in Fig. 2, nine main absorption bands are observable between 570 and 3100 cm^{-1}. The first two columns of Table 1 present the assignment of each bands. The integrated band intensities of the main bands are reported in Table 2. It can be noted that our values do not vary significantly with temperature. The only exceptions are the 570–630 cm^{-1} band and the value at 223 K of the 710–790 cm^{-1} band. The former is due to the fact that this band is at the limit of the KBr beamsplitter range. The latter may be explained by the high absorption coefficient of the Q-branch at the lowest temperature, which may have triggered a non-linear cross-section around 756.8 cm^{-1}.

Another issue with the spectrum at 223 K is the variation of the signal-to-noise ratio when the optical depth of low-pressure spectra falls below the cutoff threshold in optically thin conditions. This is due to the bands becoming more pressure-dependent as they become sharper. This triggers large variations between high- and low-pressure data. When the points corresponding to $\chi(\nu) < 0.1$ are eliminated, only the data recorded at the highest pressures and corresponding to the smoother spectra remain. This effect is particularly visible in the 770–777 cm^{-1} band. However, it only concerns the wings of the bands when the cross-sections are in the order of 10^{-19} cm^2/molecule.

Weaker bands with integrated band intensities on the order 10^{-19} cm/molecule are also reported. Some of those bands have been assigned to overtone and combination bands of the most intense fundamental vibration modes. The origin of the other bands is uncertain. For simplicity, only the integrated band intensities averaged over temperatures from 283 to 243 K have been reported in Table 3.

Table 3
Weak bands in the 570–3100 cm^{-1} spectral range. Wavenumbers are in cm^{-1} and integrated band intensities are in 10^{-19} cm/molecule.

Band	Assignment	Integrated band intensity
810–880		3.062
980–1040		2.148
1320–1360		1.884
1475–1535	$2\nu_{15}$	1.828
1640–1730	$\nu_{15}+\nu_7$	0.514
1800–1900	$2\nu_7, \nu_{15}+\nu_{14}, \nu_{15}+\nu_6$	1.772
2020–2120	$2\nu_{14}, 2\nu_6, \nu_{14}+\nu_6, \nu_5+\nu_7$	2.742
2285–2345	$2\nu_5$	1.304
2460–2580		1.716
2800–2900		1.136

5. Data validation

5.1. Comparison with literature values

Our results are compared with previously published values. Three sets of data are currently available: the spectra from Clerbaux et al. [6] (presently used in the HITRAN 2008 database [5]), the Pacific Northwest National Laboratory (PNNL) database [7], and the integrated band intensities of Orkin et al. [8].

Clerbaux et al. [6] presented three absorption spectra of a pure HCFC-141b vapour at a resolution of 0.03 cm^{-1} and temperatures of 253, 270 and 287 K over the spectral ranges 710–790, 895–955, 990–1210, and 1325–1470 cm^{-1}. The published integrated band intensity uncertainties for those bands are respectively 0.08, 0.06, 0.20 and 0.12×10^{-17} cm/molecule. The data from Clerbaux et al. [6] have been recently updated in the HITRAN database after a discrepancy was discovered in the 1325–1470 cm^{-1} region at 270 K. The corrected set is used in this publication.

The PNNL database contains three cross-section spectra of HCFC-141b broadened by a 760-Torr N_2 vapour. The spectral resolution is 0.1 cm^{-1} at 278, 298 and 323 K over the spectral range 550–6500 cm^{-1}. The uncertainty on the integrated band intensities is estimated to be lower than 2.1%.

Orkin et al. [8] presented the integrated intensities of a pure sample at 295 K over a wavenumber range of 400–1600 cm^{-1} at a resolution of 0.12 cm^{-1}. Test on a sample broadened by 650 torr of dry air was also performed. Even at this resolution, no variation of the integrated band intensities between the pure and broadened sample was reported for this molecule. The published uncertainties on the integrated intensity of the strong bands vary from 0.8 to 2%. However, the systematic uncertainty is not included.

Because all previous datasets had been recorded at different resolutions and the PNNL spectra are N_2-broadened, direct spectral comparisons were not carried out. Data validation has been performed by comparing the integrated band intensity of the main nine absorption bands between 570 and 3055 cm^{-1}. The results are reported in Table 2. Our average integrated band intensities are very consistent with the PNNL database [7] and Orkin et al. [8] for all the bands considered. However, our values show significant discrepancies at low temperatures with Ref. [6] for the 710–790, 1030–1138, and 1138–1210 bands (Fig. 3). Typically, the integrated intensities of the aforementioned bands are systematically smaller at low temperatures than the values of this present work, as well as the values of Refs. [7,8]. Traces of contamination by methanol also appear in Ref. [6] at 270 K between 990 and 1070 cm^{-1}. The integrated band intensity of Clerbaux et al. [6] at 1420–1470 cm^{-1} shows an opposite trend, with values increasing when the temperature decreases. However, in this case, Clerbaux et al. [6] values agree with the other data within their uncertainty estimates.

The absorption spectra of Ref. [7] present the same weak bands as the one reported in Table 3 of this present work. Therefore, it is extremely unlikely that our unassigned weak bands come from an experimental artefact. The hypothesis of by-products of HCFC-141b has also been rejected as the weak band intensities do not vary relatively to the strong bands when the temperature is changed.

5.2. Comparison of the integrated band intensities with theoretical calculation

Theoretical calculation was performed with the Gaussian 09 program [9]. The geometry optimization and frequency calculations of the fundamental modes were carried out ab initio with the second-order Møller–Plesset perturbation theory (MP2) and by density functional theory using Becke's three-parameter nonlocal-exchange functional of Lee–Yang–Parr (B3LYP). Different basis sets were tested for both methods (Fig. 4). Table 1 presents the calculated wavenumber and integrated band intensity of the harmonic frequencies of the best fit for both methods. All the harmonic frequency sets fit well with our main band centres. The best fit between the experimental integrated intensity of all bands, averaged over our range of temperatures, and the MP2 method was obtained with the triple-zeta correlation-consistent basis set (cc-pVTZ) giving an $R^2 = 0.98791$. Surprisingly, the simpler double-zeta correlation-consistent basis set (cc-pVDZ) was found to give the best fit for the B3LYP method with an $R^2 = 0.99402$. For both methods, the

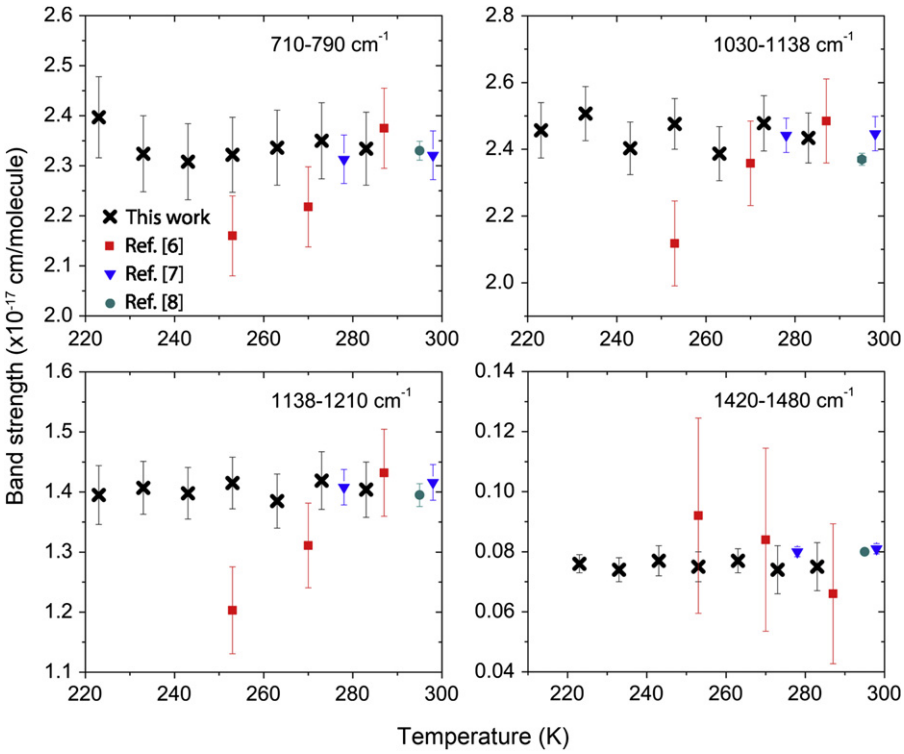

Fig. 3. Comparison of the integrated intensity of the main bands of HCFC-141b with the literature values.

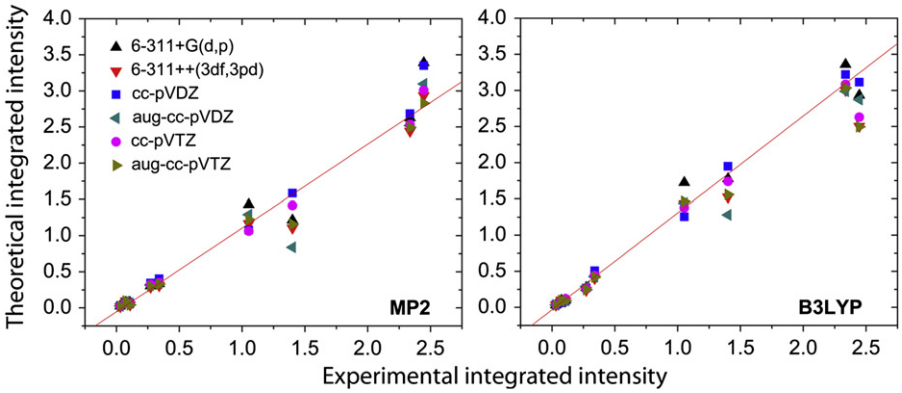

Fig. 4. Comparison between experimental and theoretical integrated band intensities for ab initio and density functional theories with multiple basis sets. Units are in $\times 10^{-17}$ cm/molecule. The lines correspond to the fit of the best basis set for each method i.e. cc-pVTZ for MP2 and cc-pVDZ for B3LYP.

integrated band intensity of the strongest bands is very sensitive to the choice of the basis set. Adding diffuse functions does not improve the result.

6. Conclusions

Cross-sections of HCFC-141b at a spectral resolution of 0.02 cm^{-1} have been reported in the mid-infrared between 560 and 3100 cm^{-1} at seven different temperatures from 223 to 283 K. The integrated cross-sections of the absorption bands agree within errors bar with Refs. [7,8]. However, important discrepancies have been found with Clerbaux et al. [6] at low temperatures. Our data have also been successfully compared to theoretical calculation performed ab initio or by density functional theory. The absorption cross-sections are available online in the supplementary data files.

Acknowledgments

This work was supported by the Natural Sciences and Engineering Research Council of Canada (NSERC) and Dr. Le Bris' startup grant from St Francis Xavier University. Computational facilities are provided by ACEnet (funded by the Canada Foundation for Innovation (CFI), the Atlantic Canada Opportunities Agency (ACOA), and the provinces of Newfoundland and Labrador, Nova Scotia, and New Brunswick).

Appendix A. Supplementary data

Supplementary data associated with this article can be found in the online version at http://dx.doi.org.10.1016/j.jqsrt.2012.05.004.

References

[1] Montzka SA, Hall BD, Elkins JW. Accelerated increases observed for hydrochlorofluorocarbons since 2004 in the global atmosphere. Geophys Res Lett 2009;36:L03804 Updated data were obtained from the National Oceanic and Atmospheric Administration (NOAA), Global Monitoring Division (GMD) web site, 24 Jan 2012, Web 24 April 2012 URL: ftp://ftp.cmdl.noaa.gov/hats/hcfcs/hcfc141b/.
[2] Brown AT, Chipperfield MP, Boone C, Wilson C, Walker KA, Bernath PF. Trends in atmospheric halogen containing gases since 2004. J Quant Spect Radio Trans 2011;112:2552–66.
[3] Toon GC, Sen B, Kleinboehl. A derivation of pseudo-lines from laboratory cross-sections. Jet Propulsion Laboratory n.d. Web 24 April 2012 URL: 〈http://mark4sun.jpl.nasa.gov/data/spec/Pseudo/Readme〉.
[4] Le Bris K, Strong K. Temperature-dependent absorption cross-sections of HCFC-142b. J Quant Spect Radio Trans 2010;111:364–71.
[5] Rothman LS, Gordon IE, Barbe A, Chris Benner D, Bernath PF, Birk M, et al. The HITRAN 2008 molecular spectroscopic database. J Quant Spect Radio Trans 2009;110:533–72.
[6] Clerbaux C, Colin R, Simon PC, Granier C. Infrared cross-sections and global warming potentials of 10 alternative hydrohalocarbons. J Geophys Res 1993;98:10491–7.
[7] Sharpe SW, Johnson TJ, Sams RL, Chu PM, Rhoderick GC, Johnson PA. Gas-phase databases for quantitative infrared spectroscopy. Appl Spectrosc 2004;58:1452–61.
[8] Orkin VL, Guschin AG, Larin IK, Huie RE, Kurylo MJ. Measurements of the infrared absorption cross-sections of haloalkanes and their use in a simplified calculational approach for estimating direct global warming potentials. J Photochem Photobio A: Chem 2003;157:211–22.
[9] Frisch MJ, Trucks GW, Schlegel HB, Scuseria GE, Robb MA, Cheeseman JR, et al. Gaussian 09. Revision A.1. Gaussian, Inc. Wallingford CT; 2009.